The Astrophysical Journal, 815:2 (10pp), 2015 December 10 doi:10.1088/0004-637X/815/1/2

RELATIVE PROPER MOTIONS IN THE RHO OPHIUCHI CLUSTER

Bruce A. Wilking[1], Frederick J. Vrba[2], and Timothy Sullivan[1]
[1] Department of Physics and Astronomy, University of Missouri–St. Louis, 1 University Boulevard, St. Louis, MO 63121, USA; bwilking@umsl.edu, tsullivan@umsl.edu
[2] U.S. Naval Observatory, 10391 West Naval Observatory Road, Flagstaff, AZ 86001-8521, USA; fjv@nofs.navy.mil
Received 2015 August 27; accepted 2015 October 14; published 2015 December 2

ABSTRACT

Near-infrared images optimized for astrometry have been obtained for four fields in the high-density L 1688 cloud core over a 12 year period. The targeted regions include deeply embedded young stellar objects (YSOs) and very low luminosity objects too faint and/or heavily veiled for spectroscopy. Relative proper motions in R.A. and decl. were computed for 111 sources and again for a subset of 65 YSOs, resulting in a mean proper motion of (0,0) for each field. Assuming each field has the same mean proper motion, YSOs in the four fields were combined to yield estimates of the velocity dispersions in R.A. and decl. that are consistent with 1.0 km s^{-1}. These values appear to be independent of the evolutionary state of the YSOs. The observed velocity dispersions are consistent with the dispersion in radial velocity derived for optically visible YSOs at the periphery of the cloud core and are consistent with virial equilibrium. The higher velocity dispersion of the YSOs in the plane of the sky relative to that of dense cores may be a consequence of stellar encounters due to dense cores and filaments fragmenting to form small groups of stars or the global collapse of the L 1688 cloud core. An analysis of the differential magnitudes of objects over the 12 year baseline has not only confirmed the near-infrared variability for 29 YSOs established by prior studies, but has also identified 18 new variability candidates. Four of these have not been previously identified as YSOs and may be newly identified cluster members.

Key words: ISM: individual objects (Rho Ophiuchi cloud) – stars: formation – stars: pre-main sequence

1. INTRODUCTION

The majority of stars in the Galaxy form in clusters that once the binding mass of the molecular gas is removed, disperse into the field population (Lada & Lada 2003). Hence, understanding the early evolution of embedded clusters will lead to a better understanding of the origin of the initial mass function, the properties of multiple-star systems, and the formation and evolution of circumstellar disks. In particular, dynamical interactions between cluster members may form the backbone of the initial mass function through processes such as competitive accretion and ejection (see the review by Bonnell et al. 2007). Encounters among young stars will also reduce the initial fraction of stars in multiple systems and must set the distribution of binary separations in field binaries (see the review by Reipurth et al. 2014). Dynamical interactions in young clusters may also affect the formation and evolution of circumstellar disks through, for example, disk truncation, and ultimately influence the formation of planetary systems (e.g., Clarke & Pringle 1993; Kobayashi & Ida 2001).

There is both observational and theoretical evidence that dynamical interactions in young clusters are important. Observations of the radial velocity dispersions of dense cores in Rho Ophiuchi, NGC 1333, and NGC 2264 range from 0.4 to 0.8 km s^{-1}, suggesting their motions are subvirial (Peretto et al. 2006; André et al. 2007; Kirk et al. 2010). These dispersions are significantly less than that of the young stars and low-density molecular gas (e.g., Foster et al. 2015; Rigliaco et al. 2015; Tobin et al. 2015). Simulations of cloud collapse and cluster evolution also indicate a higher stellar interaction rate in the embedded phase (Bate et al. 2003; Bate 2009; Proszkow & Adams 2009).

The centrally condensed L 1688 core of the Rho Ophiuchi Cloud is one of the closest regions of active low-mass star formation. It is located about 1° east of the Upper Scorpius subgroup of the Sco–Cen OB association. The L 1688 cloud contains a diverse population of >300 young stellar objects (YSOs) ranging from heavily obscured Class 0 sources to optically visible, diskless pre-main-sequence stars (see the review by Wilking et al. 2008). Distance estimates to L 1688 using *Hipparcos* distances to stars in the region are 131 ± 3 pc (Mamajek 2008) and 128 ± 8 pc (Lombardi et al. 2008). Very long baseline interferometry observations have measured parallaxes for four stars in L 1688, two at 120 pc, and two at about 165 pc with uncertainties of ∼5% (Loinard et al. 2008). We adopt a distance of 130 ± 10 pc for this study. The proximity of the cloud affords the greatest sensitivity to very low mass objects and brown dwarfs (Barsony et al. 2012). The 1 pc × 2 pc centrally condensed core exhibits very high gas column densities (A_v > 25–100 mag) and contains about 950 $M_\odot$ of molecular gas. Within the core are regions of high spatial density molecular gas associated with recent star formation as well as prestellar cores. Because of the high visual extinctions in the core, the embedded cluster is best observed at near-infrared wavelengths.

We present one of the first proper motion studies of embedded sources in the L 1688 cloud. Near-infrared images at K' obtained over a 12 year period were obtained with the goal of estimating the velocity dispersion of this young cluster. Using radio interferometry, Rivera et al. (2015) have derived absolute proper motions for three YSOs in L 1688, which allows them to estimate the mean bulk motion of the region but not the internal kinematics. Proper motion surveys have an advantage over radial velocity surveys in that perturbations due to binarity are expected to be minimal. Near-infrared proper motion surveys also have an advantage since they are sensitive to YSOs in all stages of evolution over a wide range of luminosities and are not limited in sensitivity, like infrared radial velocity surveys, due to the high extinctions and veiling.

Table 1
Proper Motion Fields in Ophiuchus

Field	R.A. (J2000)	Decl. (J2000)	Associated Core[a]	Nights Obs.
1	16:27:29.4	−24:29:19	Core B-2	19
2	16:27:31.6	−24:40:35	Core F	17
3	16:27:05.2	−24:36:10	Cores C-S, E	16
4	16:26:08.2	−24:22:45	Core A-3	16

Note.
[a] Core designations following Motte et al. (1998).

Hence, the distribution of proper motions for a young cluster can yield the velocity dispersion provided the distance is well known. We describe the data collection and reduction in Section 2, as well as the astrometric procedures to derive accurate positions and the techniques employed to derive differential magnitudes for the stellar images. Section 3 first describes the identification of variable sources, many of which have been previously identified, but several are newly identified, including possible new cluster members. The second part of Section 3 is devoted to the analysis of relative proper motions and deriving the velocity dispersion of this young cluster. Section 4 is a discussion comparing the velocity dispersion of the young cluster to that of optically visible YSOs, the low-density molecular gas, and the dense cores, and several possibilities for the relatively higher dispersion of the YSOs relative to the dense cores are explored. A brief summary is provided in Section 5.

2. OBSERVATIONS AND DATA REDUCTION

Near-infrared monitoring of infrared sources in four dense cores in the L 1688 cloud was performed at the U.S. Naval Observatory, Flagstaff Station, between 2001 and 2006 and again in 2011 and 2012. Images were obtained in the 2.1 μm K' filter using ASTROCAM mounted on the USNO 1.55 m telescope. ASTROCAM was designed for astrometry using a 1024 × 1024 ALADDIN InSb detector and employing all-reflective Offner 1:1 re-imaging optics (Fischer et al. 2003). This produces minimum field distortion over its field of view of approximately $6\farcm25 \times 6\farcm25$ with a pixel scale of $0\farcs366$ pixel^{-1}. Since 2000, ASTROCAM is used in the ongoing USNO program measuring infrared parallax and proper motion of brown dwarfs (Vrba et al. 2004; F. J. Vrba et al. 2016, in preparation) routinely producing mas and mas yr^{-1} level parallaxes and proper motions, respectively.

Three images dithered by $10''$ were obtained for each field on each night of observation, with a total co-added integration time for each dithered image of 20 minutes. The frames are processed as per the USNO infrared astrometric program by linearization via the precepts of Luginbuhl et al. (1998), flattened via dome spot lamp-on minus lamp-off flats, and sky-subtracted via sky frames produced by the mean of the dithered program using a single hi-pixel rejection.

The field centers and their corresponding dense molecular cores are summarized in Table 1. The dates of the observations for each field as well as the exposure times and number of co-adds are presented in the appendix. The location of the fields relative to infrared sources in the L 1688 cloud is shown in Figure 1.

2.1. Astrometry

Astrometry for the four fields was obtained again using the same procedures employed in both the USNO infrared and optical astrometry programs. Two important observational precepts are key to USNO astrometry. We endeavor to keep the time center of each infrared triplet observation to within ±15 minutes of time of the local meridian in order to minimize the effects of differential atmospheric refraction, even in the K' band. This procedure also makes contributions due to parallax essentially zero. Second, we carefully register each triplet set of exposures in exactly the same frame location by using differential guider offsets followed by real-time differential astrometry of pre-selected in-field stars from test frames taken before the actual science exposures. This minimizes the effects of any camera focal-plane distortions.

Astrometric centroiding employing 2D Gaussian fits is carried out on each individual processed frame for sub-rastered program sources that have been pre-selected based on their signal-to-noise ratio before any science exposures have been obtained. In-house software used in USNO astrometry (cf. Monet et al. 1992) allows almost any combination of source subsets to be examined for positions, proper motions, parallaxes, or perturbations. In the case of the Rho Ophiuchi fields, astrometric solutions for only mean positions and proper motions were allowed. We had initially hoped that enough distant background stars could be identified (from source spectral energy distributions (SEDs)) and that a reference frame could be established in each field to allow for determination of "absolute" proper motions. Unfortunately, the large opacity of the Rho Ophiuchi cores, even at the K' band, prevented this. Thus, we simply solved for the relative proper motions of sources within each field with respect to each other. While the mean proper motion of each field is zero by this method, it still allows for determining the velocity dispersion in each field, relative velocity flow distributions, and identification of outlying higher-velocity objects.

While we are confident in the astrometric results presented here, there are several potential issues we feel are worth brief discussion. The first is that at a decl. of roughly −24°, the Rho Ophiuchi clouds are observed, even on the meridian from Flagstaff at a zenith distance of approximately 60°. However, the infrared astrometric program, even though operating at shorter wavelengths (J- and H-bands), routinely determines parallaxes and proper motions of objects even several degrees farther south that are in excellent agreement with measurements from the southern hemisphere. The second issue is the effect of binarity. Most of the YSOs in this study with known spectral types, and YSOs in L 1688 in general, are low-mass stars ($M < 0.5\,M_{\odot}$; Erickson et al. 2011), and the trend for binaries in this mass range is toward equal mass systems (Goodwin 2013). In this case, we would follow the light centroid of the system without the addition of spurious proper motions. For more massive systems, the trend is toward unequal mass systems, in which case we would follow the brighter member with the smaller reflex motion. For systems with periods much shorter than our time baseline, resolved orbital motions would appear with enhanced errors in the proper motion for a given K' magnitude and that was not observed. Systems with much longer periods would not display significant orbital motion over our 12 year baseline. In summary, the effects of source decl. and binarity are expected to be minimal, and the proper

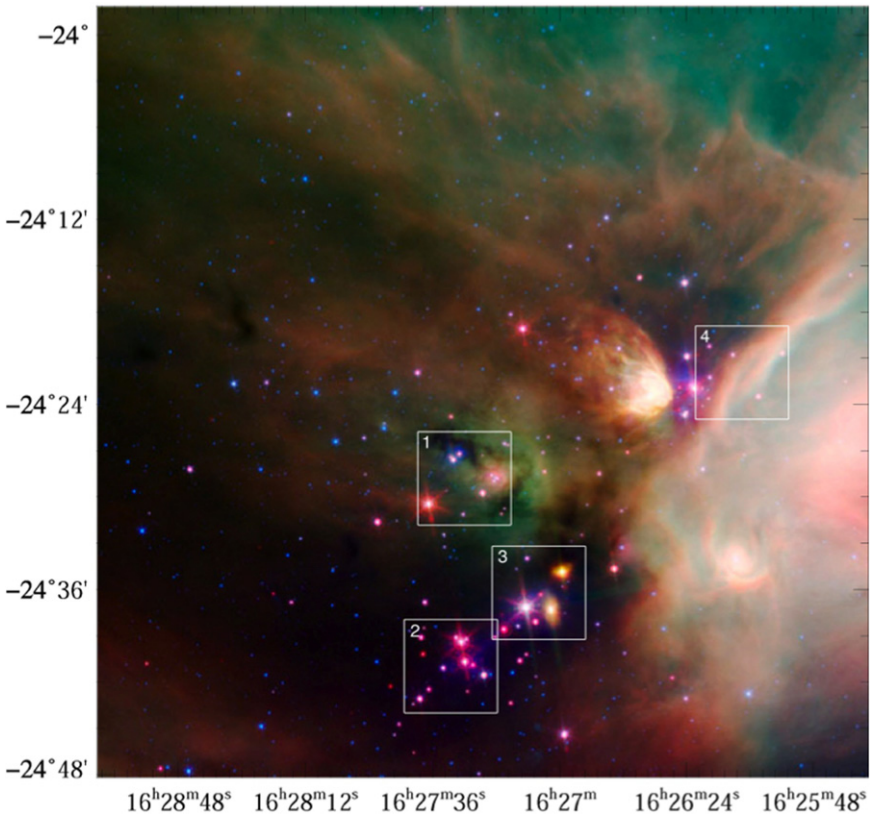

Figure 1. A combined IRAC/MIPS image of L 1688 with the red color representing emission in the MIPS 24 μm band, green the IRAC 8 μm band, and blue the IRAC 4.5 μm band (image courtesy of Robert Hurt). Numbered boxes added to indicate the fields for Core B-2 (1), Core F (2), Cores C-S and E (3), and Core A-3 (4). Class I sources appear red in color, and Class III sources and background stars appear blue. R.A. and decl. are given in J2000 coordinates.

motion errors for the Rho Ophiuchi cores are consistent with our other results, considering the brightness distribution of the sources and the time baseline of the observations.

A third, and potentially more serious concern, is that in 2006 June the original ASTROCAM camera was destroyed by a cryogenic explosion. ASTROCAM was rebuilt and returned to operation in 2011, thus explaining the unusual time distribution of observations reported here (2001–2006 and 2011–2012). The restored camera uses many of the original parts, including the detector array and the K' filter. However, a new Offner re-imager and entrance window were needed. This has the potential of introducing spurious astrometric results, no matter the care in rebuilding to exacting original specifications or differential observational techniques. In order to test for this, we first reduced the 2001–2006 data and then added the 2011 and 2012 data sets. For all fields we saw the same distribution of proper motions, albeit with reduced errors appropriate for the added observations and significantly increased time baseline. As an additional, and far more stringent test, we have continued observations of several of our parallax and proper motion brown dwarf objects which were started with the original camera. We see no systematic effects in either proper motions or parallax results when we combine the data from the two cameras. We are thus confident in the proper motion results presented here.

2.2. Differential Photometry and Variability

Aperture photometry was performed on all sources with the *phot* task in the Image Reduction and Analysis Facility (IRAF)[3] using an aperture based on the FWHM of a point source averaged over the frame (Howell 1989). Instrumental magnitudes were derived using an aperture that varied from $r = 1\farcs1$ to $1\farcs8$ with a sky annulus of $r = 3\farcs7$ with a width of $3\farcs7$. Comparison stars were identified in each of the four fields by selecting pairs of objects not known to be YSOs whose differential magnitudes did not vary significantly over the 12 year period. GY 297 and GY 303 were established as comparison stars in Field 1, GY 298, and GY 317 in Field 2; 2MASS J16271721-2435130 and J16271043-2435311 in Field 3; and 2MASS J16255557-2422173 and 2MASS J16260608-2423432 in Field 4.[4]

3. RESULTS

The 12 year baseline for these data has afforded us the opportunity to study possible near-infrared variability and measure proper motions for 111 objects in the four fields.

3.1. Confirmed and Possible New Variables

Differential magnitudes were determined for each object in each field by using one of the comparison stars from that field. The degree of variability was quantified by computing the

[3] IRAF is distributed by the National Optical Astronomy Observatory, which is operated by the Association of Universities for Research in Astronomy, Inc., under cooperative agreement with the National Science Foundation.

[4] 2MASS J16271721-2435130 was reported as a low-amplitude variable by Alves de Oliveira & Casali (2008) but was not confirmed by Parks et al. (2014) or by this study.

reduced χ^2 value given the standard deviation of the differential magnitude. This standard deviation was estimated from the quadratic sum of the uncertainties of the individual objects. Photometric uncertainties for the comparison stars were estimated by scaling up the statistical errors returned from *phot* to match the standard deviations in the differential magnitudes. Photometric uncertainties for the remaining objects were scaled from the comparison stars in proportion to their relative fluxes. Unfortunately, the irregular time-sampling of the observations do not allow us to explore the origins of the variability.

The results of our χ^2 analysis are presented in Table 2. The number of observations given in column two is not the same for all sources in a field due to edge effects or artifacts in the image unrelated to deriving accurate positional information. The last column notes comparisons to previous variability studies by Alves de Oliveira & Casali (2008), Parks et al. (2014), and Günther et al. (2014). We note that the most extensive of these was by Parks et al., who utilized nearly daily observations over a 2.5 year period from the 2MASS survey (Cutri et al. 2003). Of the 52 objects in common with the Parks et al. or Günther et al. surveys, all 29 objects for which we computed a $\chi^2 > 2$ were identified as variables in these studies. For the 24 objects with $\chi^2 < 2$, 29% (7/24) were identified as variables by these studies.

Using the criterion of $\chi^2 > 2$, we identified 18 sources with possible variability that were not included in previous variability surveys: WLY 2-48 (Field 1); GY 263, GY 295, GY 310, J16273955-24433171, WLY 2-51, J16274160-24383830, GY 323, GMM 136, GY 326, and WLY 2-53 (Field 2); and SR 4, SKS 1-2, C81 8, DoAr 21/GSS 23, GSS 26, SKS 1-7, and GSS 28 (Field 4). Four of these objects, WLY 2-53, J16273955-2443317, and J16274160-24383830 (Field 2), and SKS 1-2 (Field 4) had not been previously identified as YSOs and are possible association members.

3.2. Relative Proper Motions

We first computed relative proper motions for all 111 sources in each of the four fields whereby the mean proper motion for each field is naturally 0 mas yr^{-1} in both R.A. and decl. Table 3 lists these values in units of mas yr^{-1} for the 46 objects not known to be YSOs. From this analysis, several objects stood out with significantly higher proper motions.

3.2.1. High Proper Motion Objects

Five objects displayed proper motions significantly greater than the average of the absolute values in R.A. or decl. None have been identified with any signatures of youth such as X-ray emission or an infrared excess. In Field 1, GY 297 is a visible ($R = 14.7$), relatively unobscured M2 star with an estimated visual extinction of $A_v = 1.3$ mag (Wilking et al. 2005). It has a significantly higher proper motion in R.A. than the mean (> 60 mas yr^{-1}). This, coupled with the lack of any signature of youth and the low extinction, suggests it is a foreground object. 2MASS J16273288-2428116 has a a marginally higher proper motion in R.A. (18 mas yr^{-1}) than the average of sources in Field 1 if GY 297 is removed. It was identified as a brown dwarf candidate (object 1307; Marsh et al. 2010a), but model fits to its low-resolution spectrum indicate it is a background star with $A_v = 36$ mag (Marsh et al. 2010b).

Table 2
Objects Displaying Variability

Source Name[a]	No. of Obs.	$\Delta K'$	$\sigma(K')$	Previous ID[b]
Field 1				
GY 236	55	0.34	0.04	(1), (3)
GY 239	56	0.20	0.03	(1), (2), (3)
GY 238	50	0.55	0.09	(1), (2)
GY 244	50	0.93	0.04	(2), (3)
WL 4	50	0.62	0.02	(2), (3)
WL 3	50	0.32	0.03	(3)
WL 6	50	1.1	0.03	(1), (2), (3)
GY 264	55	0.44	0.03	(1), (2), (3)
WL 13	56	0.28	0.02	(2), (3)
VSSG 18	56	0.46	0.02	(3)
VSSG 17	56	0.18	0.02	(2)
WLY 2-48	56	0.34	0.02	⋯
Field 2				
GY 245	51	0.77	0.03	(2)
SR 12	45	0.21	0.03	(2)
WLY 2-42	45	0.29	0.03	(2)
GY 253	44	0.22	0.03	(1), (2)
ISO-Oph 137	45	1.1	0.04	(2), (3)
GY 262	51	0.59	0.03	(2), (3)
GY 263	45	0.46	0.03	⋯
WLY 2-43	45	0.53	0.03	(2), (3)
WLY 2-44	51	1.6	0.03	(2), (3)
WLY 2-46	51	2.0	0.03	(2), (3)
GY 292	51	0.37	0.03	(3)
GY 295	51	0.23	0.03	⋯
GY 301	51	0.71	0.03	(3)
GY 310	51	0.24	0.03	⋯
GY 312	51	0.52	0.03	(3)
GY 314	51	0.34	0.03	(3)
J16273955-24433171	39	0.39	0.07	⋯
WLY 2-51	51	0.44	0.03	⋯
J16274160-24383830	51	1.1	0.11	⋯
GY 323	51	0.32	0.03	⋯
GMM 136	50	1.0	0.11	⋯
GY 326	51	0.22	0.03	⋯
WLY 2-53	42	0.28	0.03	⋯
Field 3				
WL 14	43	1.0	0.13	(2), (3)
WL 17	43	1.6	0.13	(1), (2), (3)
EL 29	43	1.4	0.13	(1), (3)
WL 11	43	1.4	0.13	(1), (2), (3)
Field 4				
SR 4	41	0.65	0.05	⋯
SKS 1-2	41	0.41	0.05	⋯
C81 8	41	0.44	0.05	⋯
DoAr 21/GSS 23	41	0.56	0.05	⋯
GSS 26	41	1.2	0.05	⋯
SKS 1-7	33	0.44	0.05	⋯
GSS 29	41	0.47	0.05	(3)
GSS 28	41	0.54	0.05	⋯
CRBR 12	41	1.8	0.05	(3)
CRBR 15	41	0.89	0.05	(3)

Notes.
[a] Source names from optical studies by (SR) Struve & Rudkjobing (1949), (DoAr) Dolidze & Arakelyan (1959), (C81) Chini (1981) and infrared studies by (GSS) Grasdalen et al. (1973), (VSSG) Vrba et al. (1975), (EL) Elias (1978), (WL) Wilking & Lada (1983), (WLY) Wilking et al. (1989), (GY) Greene & Young (1992), (CRBR) Comeron et al. (1993), (SKS) Strom et al. (1995), (ISO-Oph) Bontemps et al. (2001), (GMM) Gutermuth et al. (2009).
[b] Previously identified as variable by (1) Alves de Oliveira & Casali (2008), (2) Parks et al. (2014), or (3) Günther et al. (2014).

Table 3
Proper Motions for Non-YSOs Relative to All Sources in Field

Source Name[a]	R.A.(J2000) (hhmmss.s)	Decl.(J2000) (° ′ ″)	J (mag)	H (mag)	K'[b] (mag)	$\mu_\alpha \cos\delta$ (mas yr^{-1})	μ_δ (mas yr^{-1})
Field 1							
	16 27 22.1	−24 27 11.3	⋯	⋯	15.8[c]	−10.93 ± 2.14	−3.80 ± 3.88
	16 27 26.9	−24 31 10.5	⋯	⋯	15.2[c]	−0.20 ± 1.92	−16.18 ± 2.46
GY 272	16 27 28.14	−24 31 43.09	<17.3	16.25	13.71	1.38 ± 0.77	−7.82 ± 0.92
	16 27 29.60	−24 29 24.77	<18.4	<17.1	14.30	−2.60 ± 1.41	−2.22 ± 1.20
	16 27 30.6	−24 30 38.3	⋯	⋯	15.5[c]	8.06 ± 2.96	−16.61 ± 2.49
	16 27 30.77	−24 29 13.62	<18.7	<16.5	14.88	0.88 ± 1.91	−16.93 ± 1.22
	16 27 32.88	−24 28 11.68	<17.8	<16.6	14.88	18.20 ± 1.80	4.90 ± 1.68
	16 27 36.21	−24 30 20.28	<16.7	<15.8	14.97	−15.98 ± 1.76	3.95 ± 1.77
GY 297	16 27 36.52	−24 28 33.28	11.99	11.38	11.15	62.63 ± 0.74	−5.32 ± 0.53
	16 27 36.53	−24 29 29.79	<17.8	16.23	14.20	−5.66 ± 1.11	−9.50 ± 1.28
GY 303	16 27 37.11	−24 28 45.70	<16.8	14.45	12.78	−2.34 ± 0.77	−9.90 ± 0.72
	16 27 38.9	−24 28 31.6	⋯	⋯	14.9[c]	−12.27 ± 4.91	−9.98 ± 2.87
GY 313	16 27 38.94	−24 30 24.56	<18.4	15.42	14.07	3.10 ± 1.15	−5.22 ± 1.38
	16 27 39.5	−24 30 34.4	⋯	⋯	15.1[c]	−1.61 ± 3.31	−2.42 ± 2.65
	16 27 39.96	−24 31 27.42	<17.4	15.23	13.50	−4.90 ± 0.93	−4.63 ± 0.70
Field 2							
	16 27 19.7	−24 41 48.	⋯	⋯	14.5[c]	−1.11 ± 2.23	1.33 ± 2.07
	16 27 31.53	−24 38 24.86	<18.7	16.21	15.16	7.67 ± 1.83	−9.01 ± 2.04
	16 27 31.63	−24 37 54.40	<17.4	15.47	14.36	0.34 ± 1.02	−3.53 ± 0.92
	16 27 33.18	−24 40 36.10	<18.6	16.36	14.38	7.59 ± 0.88	−18.82 ± 1.28
	16 27 35.34	−24 39 58.32	<18.6	16.63	15.00	3.29 ± 1.72	−10.89 ± 2.34
GY 298	16 27 36.81	−24 39 39.21	<16.8	14.98	13.62	−6.17 ± 0.80	−9.89 ± 0.91
	16 27 36.98	−24 42 01.79	<17.4	<17.8	14.84	6.24 ± 1.39	−9.47 ± 1.53
	16 27 37.82	−24 38 45.70	<18.1	16.27	14.68	0.66 ± 1.27	−9.63 ± 1.58
	16 27 38.05	−24 38 25.40	<17.5	16.19	15.22	3.23 ± 1.89	−7.08 ± 2.29
	16 27 39.55	−24 43 31.71	<18.7	<15.5	14.57	−8.29 ± 1.49	−21.57 ± 1.30
	16 27 39.6	−24 39 04.5	⋯	⋯	14.1[c]	−8.48 ± 1.56	−4.69 ± 2.04
AOC 85	16 27 39.9	−24 38 51.3	⋯	15.41[d]	14.06[d]	1.94 ± 0.96	−0.19 ± 0.76
GY 317	16 27 40.10	−24 38 36.46	16.97	14.72	13.47	6.44 ± 0.88	−14.80 ± 0.89
	16 27 41.60	−24 38 38.30	⋯	15.85	15.11	−2.62 ± 1.33	−6.95 ± 1.87
	16 27 43.3	−24 38 49.4	⋯	⋯	15.5[c]	−1.62 ± 2.45	−9.46 ± 3.92
WLY 2-53	16 27 43.78	−24 43 08.05	<17.8	13.75	11.14	−1.61 ± 0.80	−9.08 ± 0.77
Field 3							
	16 27 05.9	−24 37 08.5	⋯	⋯	15.4[c]	−6.17 ± 4.19	−2.43 ± 4.78
	16 27 10.4	−24 35 31.4	⋯	⋯	15.4[c]	−1.18 ± 2.61	-13.15 ± 2.29
	16 27 14.5	−24 34 57.6	⋯	⋯	15.5[c]	8.94 ± 2.68	-13.89 ± 2.52
AOC 67	16 27 17.21	−24 35 13.05	<17.6	16.26	14.52	−0.01 ± 1.22	−3.50 ± 1.60
Field 4							
	16 25 55.50	−24 22 17.34	<18.3	15.73	14.51	−1.04 ± 1.53	15.75 ± 1.91
SKS 3-3	16 25 56.74	−24 23 32.28	<18.7	14.85	13.25	−33.65 ± 0.55	44.74 ± 0.80
	16 25 57.10	−24 23 17.81	<18.7	15.68	14.62	5.48 ± 0.99	−13.37 ± 2.54
SKS 1-2	16 25 58.57	−24 22 01.89	15.23	12.64	11.33	3.02 ± 0.50	−12.72 ± 0.81
	16 25 58.87	−24 23 56.45	<17.8	15.47	14.40	5.28 ± 1.23	−18.71 ± 1.91
	16 26 01.09	−24 23 33.33	<16.0	16.35	14.32	5.34 ± 1.64	−16.60 ± 3.03
	16 26 01.69	−24 23 28.86	<15.8	<14.6	14.88	16.40 ± 1.60	−17.86 ± 2.14
CRBR 1	16 26 05.00	−24 24 49.97	<18.6	15.81	14.08	6.75 ± 1.37	−6.17 ± 3.54
CRBR 2	16 26 06.09	−24 23 43.21	<16.1	15.69	14.22	0.87 ± 1.83	−8.12 ± 1.16
	16 26 07.03	−24 19 26.52	<18.5	<17.5	14.84	3.19 ± 1.10	−15.02 ± 1.66
CRBR 7	16 26 12.71	−24 22 39.98	<18.3	<17.5	13.99	3.26 ± 0.85	−13.83 ± 1.07

Notes.
[a] Sources names from infrared studies by (WLY) Wilking et al. (1989), (GY) Greene & Young (1992), (CRBR) Comeron et al. (1993), (SKS) Strom et al. (1995), and (AOC) Alves de Oliveira & Casali (2008).
[b] Positions and near-infrared magnitudes are from the 2MASS survey (Cutri et al. 2003), except where noted.
[c] Positions and photometry estimated from differential magnitudes with non-variable sources are from this study.
[d] Photometry from Alves de Oliveira & Casali (2008).

2MASS J16255674-2423323 (SKS 3-3) in Field 4 has no optical counterparts and no signature of youth. It displays proper motions in R.A. and decl. of −34 mas yr^{-1} and 45 mas yr^{-1}, respectively. Estimates for its visual extinction vary from 11 to 24 mag, depending on whether it is an early- or late-type star. While it is clearly not a foreground star, detections in only the H and K bands render its true nature poorly constrained. The two remaining objects, 2MASS J16260169-2423288 (Field 4) and 2MASS J16273955-2443317 (Field 2), are relatively faint with detections only in K' (14.88 and 14.57, respectively).

Table 4
Proper Motions for YSOs Relative to YSOs in Field

Source Name[a]	Other Name	R.A.(J2000) (hhmmss.s)	Decl.(J2000) (° ′ ″)	J (mag)	H (mag)	K'[b] (mag)	SED Class[c]	$\mu_\alpha \cos\delta$ (mas yr^{-1})	μ_δ (mas yr^{-1})
Field 1									
GY 236	WLY 2-33	16 27 14.51	−24 26 46.10	<18.6	15.34	12.26	1/2	−0.46 ± 0.69	0.46 ± 0.57
GY 239	WLY 2-34	16 27 15.45	−24 26 39.80	17.42	13.46	10.79	F/2	−0.15 ± 0.51	0.11 ± 0.39
GY 238	WLY 2-35	16 27 15.51	−24 30 53.70	<18.0	16.19	12.79	F	−2.62 ± 0.77	0.57 ± 0.99
GMM 110	IKT 30	16 27 16.44	−24 31 14.50	<18.7	<17.7	15.09	1/F	0.11 ± 2.27	−1.41 ± 3.23
GY 244	WLY 2-37	16 27 17.57	−24 28 56.30	<17.2	14.42	11.58	1/F	4.59 ± 2.52	0.35 ± 0.88
WL 5	GY 246	16 27 18.17	−24 28 52.70	<17.9	14.68	10.56	3	−1.23 ± 0.46	−2.83 ± 0.88
WL 4	GY 247	16 27 18.49	−24 29 05.90	14.61	11.50	9.68	2	−1.73 ± 0.76	−0.03 ± 0.50
WL 3	GY 249	16 27 19.22	−24 28 43.90	<17.6	14.66	11.49	1/F	1.14 ± 0.45	−1.77 ± 0.78
GY 254	WL 6	16 27 21.80	−24 29 53.40	<18.6	15.38	10.83	1/F	0.53 ± 0.65	−2.00 ± 0.66
GMM 147	⋯	16 27 21.83	−24 27 27.58	<17.7	<17.7	14.51	F	−0.12 ± 1.14	1.89 ± 1.08
GY 256	GMM 114	16 27 21.98	−24 29 39.80	<18.7	15.43	12.79	2	−0.04 ± 0.54	−2.65 ± 0.49
GY 257	IKT 48	16 27 24.20	−24 29 29.50	<17.6	14.99	12.33	3	1.65 ± 0.53	2.41 ± 0.42
GY 259	IKT 50	16 27 24.64	−24 29 35.40	<18.7	14.78	12.43	3	2.60 ± 0.42	2.91 ± 0.51
GY 264	IKT 52	16 27 26.58	−24 25 54.40	13.00	12.35	11.84	2	−0.41 ± 0.61	−1.08 ± 0.80
WL 13	GY 267	16 27 27.38	−24 31 16.60	12.35	10.38	9.32	2	−0.04 ± 0.43	1.69 ± 0.69
VSSG 18	GY 273	16 27 28.45	−24 27 21.00	15.74	12.31	10.10	F	−1.53 ± 0.62	−1.37 ± 0.78
VSSG 17	GY 279	16 27 30.18	−24 27 43.40	15.32	11.52	9.02	F/2	0.65 ± 0.43	−1.68 ± 0.42
ISO-Oph 150	GMM 28	16 27 30.91	−24 27 33.19	<18.0	<16.7	14.86	1	−2.73 ± 2.10	4.87 ± 2.34
GY 287	GMM 123	16 27 32.14	−24 29 43.58	<18.4	15.03	13.04	2	−0.74 ± 0.42	2.88 ± 0.58
WLY 2-48	GY 304	16 27 37.19	−24 30 35.00	10.57	8.82	7.58	2	−2.12 ± 0.46	−2.55 ± 0.47
GY 306	WLY 2-50	16 27 38.13	−24 30 42.90	12.50	10.54	9.66	3	1.45 ± 0.91	−1.04 ± 0.97
GMM 132	SKS 3-65	16 27 40.10	−24 26 36.50	<18.6	<16.5	14.10	2	1.30 ± 1.07	−0.89 ± 0.99
Field 2									
GY 245	GMM 21	16 27 18.38	−24 39 14.70	<18.7	15.54	12.23	F	0.34 ± 0.74	0.32 ± 0.91
SR 12	GY 250	16 27 19.51	−24 41 40.40	9.42	8.63	8.40	3	−0.95 ± 0.31	2.02 ± 0.45
WLY 2-42	GY 252	16 27 21.47	−24 41 43.10	15.22	11.25	8.48	F/2	−0.36 ± 0.42	0.16 ± 0.45
GY 253	SKS 3-39	16 27 21.83	−24 43 35.69	17.27	13.20	10.77	3	0.28 ± 0.43	−0.34 ± 0.60
GY 258	ISO-Oph 136	16 27 24.39	−24 41 47.60	<17.1	14.93	12.72	3	0.72 ± 0.61	0.20 ± 0.62
ISO-Oph 137	GMM 23	16 27 24.61	−24 41 03.40	<17.7	<16.6	13.68	1	1.24 ± 1.34	−1.79 ± 2.02
GY 260	GMM 24	16 27 26.29	−24 42 46.10	<17.8	15.18	12.66	F	1.20 ± 0.43	−0.24 ± 0.84
GY 262	GMM 117	16 27 26.49	−24 39 23.10	15.69	12.07	9.95	2	1.26 ± 0.36	−1.54 ± 0.61
GY 263	SKS 3-48	16 27 26.62	−24 40 45.16	<18.6	15.47	12.78	F	1.92 ± 1.34	−1.12 ± 2.41
WLY 2-43	GY 265	16 27 26.94	−24 40 50.80	<18.5	13.52	9.74	1	−3.05 ± 0.78	1.91 ± 0.56
WLY 2-44	GY 269	16 27 28.03	−24 39 33.50	<16.6	13.68	10.38	1	−4.00 ± 2.14	0.76 ± 0.93
WLY 2-46	GY 274	16 27 29.44	−24 39 16.20	16.72	12.64	9.84	1/F	0.04 ± 0.45	0.53 ± 0.47
GY 292	GMM 126	16 27 33.11	−24 41 15.30	11.32	9.13	7.81	2	−0.20 ± 0.31	−0.88 ± 0.39
GY 295	IKT 70	16 27 35.26	−24 38 33.40	11.28	10.23	9.67	3	0.88 ± 0.47	−0.68 ± 0.47
GY 301	GMM 127	16 27 37.25	−24 42 38.00	<18.7	14.52	11.46	F	1.81 ± 0.51	0.80 ± 0.64
GY 310	GMM 129	16 27 38.63	−24 38 39.20	13.27	11.93	11.08	2/F	−1.03 ± 0.38	0.19 ± 0.53
GY 312	GMM 31	16 27 38.94	−24 40 20.70	16.54	13.91	12.29	1	0.72 ± 0.51	−3.33 ± 1.06
GY 314	GMM 130	16 27 39.43	−24 39 15.50	10.75	9.21	8.46	2/F	1.19 ± 0.36	−0.50 ± 0.42
WLY 2-51	GY 315	16 27 39.83	−24 43 15.10	17.05	12.13	8.99	2/F	0.41 ± 0.49	−1.25 ± 0.65
GY 323	GMM 135	16 27 41.75	−24 43 36.10	<18.5	14.88	12.29	F/2	−2.30 ± 0.65	−2.15 ± 0.96
GMM 136	⋯	16 27 41.79	−24 42 34.60	<18.5	<17.2	15.11	2	−0.49 ± 2.03	4.74 ± 2.42
GY 326	GMM 137	16 27 42.70	−24 38 50.60	13.24	11.44	10.54	2	0.28 ± 0.49	2.12 ± 0.47
Field 3									
WL 21	GY 164	16 26 57.33	−24 39 14.70	<18.2	15.09	12.81	2	0.30 ± 0.58	−0.35 ± 0.54
CRBR 51	GMM 81	16 26 58.28	−24 41 40.40	<18.2	<16.7	14.41	2	1.14 ± 1.22	−0.51 ± 1.02
WL 14	GY 172	16 26 59.05	−24 41 43.10	16.05	13.35	11.82	2	0.42 ± 0.64	0.92 ± 0.54
WL 16	GY 182	16 27 02.34	−24 41 47.60	14.16	10.48	8.06	1	0.34 ± 0.41	−0.76 ± 0.35
GY 197	GMM 16	16 27 05.25	−24 41 03.40	<18.6	<16.4	14.44	1	−2.15 ± 2.08	−1.92 ± 1.56
GY 201	⋯	16 27 06.04	−24 39 23.10	15.86	15.12	14.62	1	−1.20 ± 1.41	0.34 ± 0.97
WL 17	GY 205	16 27 06.78	−24 40 45.16	<17.3	14.30	10.97	F	−0.66 ± 0.62	2.07 ± 0.50
WL 10	GY 211	16 27 09.10	−24 40 50.80	12.55	10.19	8.92	2	−0.93 ± 0.53	0.50 ± 0.47
EL 29	GY 214	16 27 09.43	−24 39 33.50	16.79	11.05	7.14	1	0.53 ± 0.68	0.04 ± 0.45
WL 19	GY 227	16 27 11.71	−24 41 15.30	<18.6	15.06	11.06	1/2	0.91 ± 0.58	−0.91 ± 0.65
WL 11	GY 229	16 27 12.13	−24 38 33.40	15.62	13.11	11.49	2	1.22 ± 0.49	0.01 ± 0.57
Field 4									
SR 4	ISO-Oph 6	16 25 56.16	−24 20 48.20	9.15	8.14	7.52	2	1.58 ± 0.62	1.58 ± 0.73
SKS 1-2	GMM 34	16 25 57.70	−24 23 18.23	<18.3	14.88	13.18	⋯	3.45 ± 0.61	−1.19 ± 0.53
C81 8	ROXRA 8	16 25 59.65	−24 21 22.30	10.67	9.95	9.53	3	1.52 ± 0.49	1.10 ± 0.49
DoAr 21/GSS 23	GMM 36	16 26 03.02	−24 23 36.00	8.09	6.86	6.23	3	−8.92 ± 0.54	−1.24 ± 0.60

Table 4
(Continued)

Source Name[a]	Other Name	R.A.(J2000) (hhmmss.s)	Decl.(J2000) (° ′ ″)	J (mag)	H (mag)	K'[b] (mag)	SED Class[c]	$\mu_\alpha \cos\delta$ (mas yr^{-1})	μ_δ (mas yr^{-1})
GSS 26	GMM 40	16 26 10.33	−24 20 54.80	14.37	10.85	8.48	2	1.64 ± 0.23	−0.51 ± 0.61
SKS 1-7	GDS J162615.8-241922	16 26 15.81	−24 19 22.10	14.03	11.40	10.03	3	−3.54 ± 0.32	−2.61 ± 1.23
GSS 29	GMM 41	16 26 16.84	−24 22 23.20	11.02	9.13	8.20	2	2.41 ± 0.78	0.81 ± 0.89
GSS 28	ISO-Oph 20	16 26 17.06	−24 20 21.60	9.66	8.61	8.06	2	−0.11 ± 0.26	1.62 ± 0.78
CRBR 12	GMM 1	16 26 17.23	−24 23 45.40	<17.6	15.46	12.25	1	0.47 ± 1.11	−0.24 ± 1.10
CRBR 15	GMM 46	16 26 18.98	−24 24 14.30	16.11	13.75	11.94	F/2	1.68 ± 1.95	0.76 ± 1.99

Notes.
[a] Sources names from optical studies by (SR) Struve & Rudkjobing (1949), (DoAr) Dolidze & Arakelyan (1959), (C81) Chini (1981); infrared studies by (GSS) Grasdalen et al. (1973), (VSSG) Vrba et al. (1975), (EL) Elias (1978), (WL) Wilking & Lada (1983), (WLY) Wilking et al. (1989), (GY) Greene & Young (1992), (CRBR) Comeron et al. (1993), (SKS) Strom et al. (1995), (ISO-Oph) Bontemps et al. (2001), (GMM) Gutermuth et al. (2009); and X-ray surveys by (ROXRA) Grosso et al. (2000), (IKT) Imanishi et al. (2001), (GDS) Gagné et al. (2004).
[b] Near-infrared magnitudes are from the 2MASS survey (Cutri et al. 2003).
[c] Spectral energy distribution class as defined by the slope of mid-infrared photometry from 3.6 to 8.0 μm and/or the spectral index from 2.2 to 24 μm.

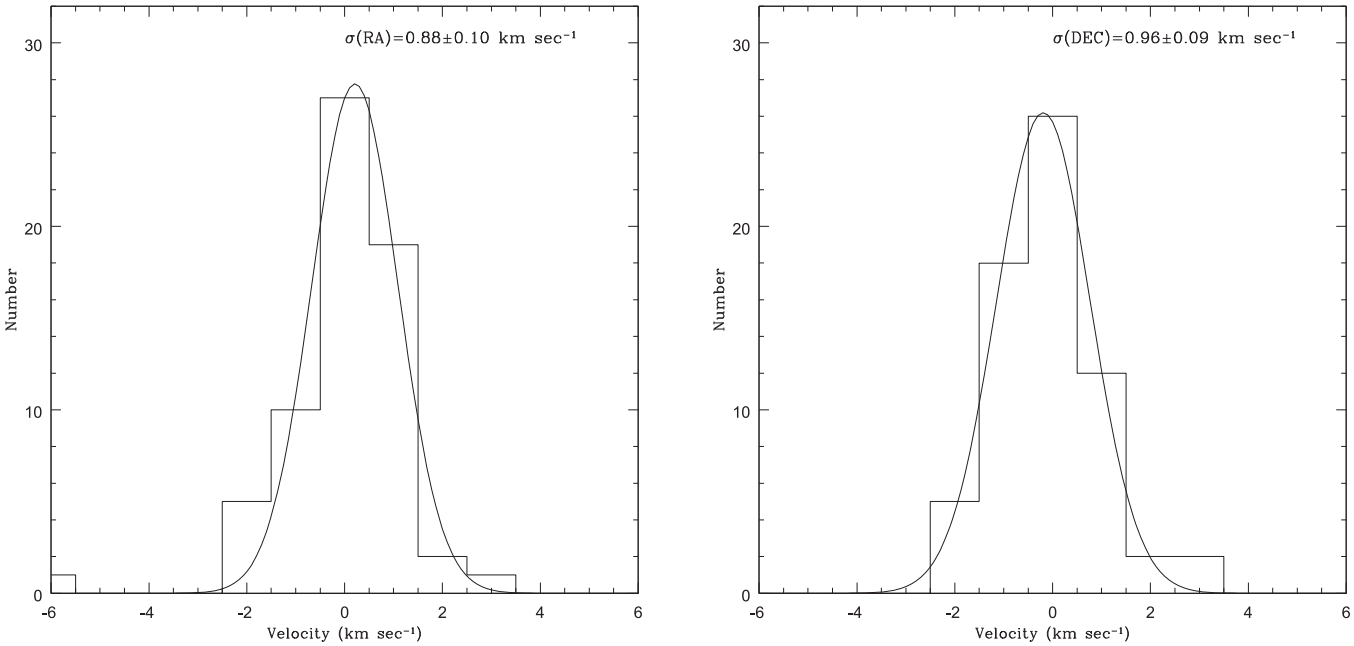

Figure 2. Velocity dispersion in R.A. (left) and decl. (right) combining the relative proper motions from all fields.

Table 5
Velocity Dispersions from Relative Proper Motions

Sample	No. of Sources	$\Delta v_{\rm R.A.}$ (km s^{-1})	$\Delta v_{\rm Decl.}$ (km s^{-1})
Fields 1 and 2	44	0.82 ± 0.10	0.97 ± 0.10
All Fields	65	0.88 ± 0.10	0.96 ± 0.09
SED Class I, F	29/26	0.84 ± 0.11	0.71 ± 0.09
SED Class II, III	28	0.88 ± 0.08	1.28 ± 0.26

3.2.2. Velocity Dispersions

Solutions were rerun for the relative proper motions, including only the 65 objects known to be YSOs. These values are presented in the last two columns of Table 4 in units of mas yr^{-1}, along with their positions and infrared magnitudes. Median uncertainties were 0.60 mas yr^{-1} in R.A. and 0.71 mas yr^{-1} in decl. or 0.37 km s^{-1} and 0.44 km s^{-1}, respectively, at the distance to the Rho Ophiuchi cloud. Gaussian fits to the velocity dispersions in R.A. and decl. are presented in Table 5 for Fields 1 and 2 combined (which contain 68% of the sources in this study or 44 sources) and all fields combined (65 sources), again assuming all fields had the same mean relative proper motion. In the latter case, histograms of the velocity dispersions are shown in Figure 2 with the best-fit Gaussians. The quoted uncertainty includes a distance uncertainty of 0.08 added in quadrature to the error in the Gaussian fit. The one-dimensional velocity dispersion in R. A. and decl. are consistent within the uncertainties of the fits with an average of $\Delta v_{\rm 1D} = 1.0$ km s^{-1}.

To examine the possibility that the velocity dispersions are dependent on evolutionary state, we characterized the infrared excess from the SED of each YSO from a least squares fit to the slope α of the log λF_λ flux densities from 3.6 to 8.0 μm. Flux

densities were compiled from the *Spitzer* c2d catalog available in the NASA/IPAC Infrared Science Archive. The sample was then divided equally into YSOs with excesses representative of Class I or Flat SEDs ($\alpha > -0.6$) and those with Class II/III SEDs ($\alpha < -0.6$). Sources with proper motion uncertainties greater than 1 km s^{-1} were excluded from this analysis. The results are summarized in Table 5. Although the sample sizes are smaller, the velocity dispersions are again consistent with $\Delta v_{1D} = 1.0$ km s^{-1} with no apparent dependence on evolutionary state for YSOs detectable in the near infrared.

4. DISCUSSION

The one-dimensional velocity dispersion of our sample derived from relative proper motions is consistent with $\Delta v_{1D} = 1.0$ km s^{-1} in both R.A. and decl. Unlike radial velocity surveys, there is no correction needed for the effects of unresolved binaries since the long time baseline of the observations should follow the barycenters of the systems. The velocity dispersions in the plane of the sky are comparable to the radial velocity dispersions observed for optically visible YSOs and the low-density molecular gas. As part of the *Gaia*-ESO optical spectroscopic survey of star-forming regions, Rigliaco et al. (2015) obtained high-resolution optical spectra for over 200 objects and derived an intrinsic radial velocity dispersion for 50 YSOs in L 1688 of 1.14 ± 0.35 km s^{-1}. The average velocity dispersion in the low-density ^{13}CO gas in which most of our sources reside is 1.06 km s^{-1} (clump R22; Loren 1989a).

The observed velocity dispersions are consistent with virial equilibrium. The one-dimensional velocity dispersion for a cluster in virial equilibrium, ignoring effects of external pressure and magnetic fields, is given by

$$\Delta v_{1D} = (GM/5R)^{1/2}.$$

Since most of the binding mass is in the molecular gas, M is the mass and R is the radius of the L 1688 cloud core. Using maps of ^{13}CO column density computed assuming a constant excitation temperature of 25 K (Loren 1989b) and a ratio of $N(H_2)/N(^{13}CO) = 4.0 \times 10^5$ (Pineda et al. 2008), we derive a total mass of 950 ± 325 $M_\odot$ for the 0.60 ± 0.07 pc radius core of the L 1688 cloud assuming a distance of 130 pc. This value for the core radius is derived from the geometric mean of the major and minor axes of the elliptical core. In deriving the mass uncertainty, we have assumed errors of 30% in the column densities, 25% in the $N(H_2)/N(^{13}CO)$ ratio and an uncertainty of ± 10 pc for the distance to the cloud. Using these values, the one-dimensional velocity dispersion in virial equilibrium would be 1.2 ± 0.2 km s^{-1}.

While the observed velocity dispersions are consistent with virial equilibrium, they are significantly higher than the radial velocity dispersion of the prestellar condensations that reside in the L 1688 cloud core. Based on N_2H^+ (1-0) observations, André et al. (2007) measured a radial velocity dispersion of 0.36 km s^{-1} for 41 prestellar condensations and 3 protostars in L 1688. After subtracting the velocity gradient observed across L 1688, the one-dimensional velocity dispersion was reduced to 0.25 km s^{-1}. This led André et al. to suggest that the dense cores formed in subvirial conditions. A similar relationship between the radial velocity dispersion of the YSOs and dense cores has been observed in the NGC 1333 cluster (Foster et al. 2015). Given a YSO crossing time of $\sim 5 \times 10^5$ years and the embedded nature of many of the YSOs in this study, it is difficult to understand how stellar encounters could account for this difference.

In the current paradigm of star formation, dense cores form in velocity-coherent filamentary clouds formed from converging turbulent flows (e.g., Elmegreen 2007; Gong & Ostriker 2011). It has been proposed that the higher velocity dispersion of the YSOs could arise due to magnetic fields constraining the dense cores or the global collapse of the cluster that would convert gravitational potential energy to kinetic energy and thereby increase the probability of stellar encounters (André et al. 2007; Foster et al. 2015). In the former case, it is not clear that magnetic fields have sufficient strength or geometry in L 1688 to affect core dynamics. For the magnetic field to influence the core dynamics, the magnetic energy would have to be comparable to the potential energy of the cluster. Given the potential energy defined by the low-density gas of $|W| = 8 \times 10^{46}$ erg, the magnetic field strength would need to be $B = \sqrt{6|W|R^{-3}} \approx 300$ μG. While this value is likely an upper limit, it is significantly higher than one would estimate by scaling the magnetic field to the average density of the low-density gas. For example, using the scaling relation of Crutcher (2012) and an average gas density of 1×10^4 cm^{-3}, one would predict a magnetic field strength of $B = 100$ μG. Moreover, near-infrared polarimetry of sources toward L 1688 indicate the magnetic field is distorted in the vicinity of the cloud core and that the star formation is proceeding supercritically (Vrba et al. 1976; Vrba 1977; Tamura et al. 2011). In the second case, to explain the higher velocity dispersion of the cluster, it is plausible that a global collapse is occurring. Several lines of evidence point to an external trigger for star formation in L 1688, including the elongation of the high column density cloud core and geometry of the cloud "streamers" perpendicular to this elongation point. A shock wave from the Upper Scorpius OB subgroup has been proposed to provide the external pressure to compress the gas to higher densities and initiate star formation (Vrba 1977; Loren 1989b; de Geus 1992; Preibisch & Zinnecker 1999). Absent an external trigger, hydrodynamical simulations of clouds with decaying turbulence suggest that stars may form in filaments and then fall in toward the gravitational well of the dense gas (e.g., Bate et al. 2003; Bate 2009). In short, the formation of multiple stars in a fragmenting dense core will naturally lead to increase stellar interactions and a higher velocity dispersion relative to the dense gas (see also Guszejnov & Hopkins 2015).

5. SUMMARY

We have obtained near-infrared images of 4 fields in the high-density L 1688 cloud core over a 12 year period. The targeted regions include deeply embedded YSOs and very low luminosity objects that may not be accessible with spectroscopy. Relative proper motions in R.A. and decl. were computed for 65 YSOs whereby the mean proper motion in each field is (0,0) mas yr^{-1}. Velocity dispersions in R.A. and decl. were found to be consistent with 1.0 km s^{-1}. These values appear independent of the evolutionary state of the YSOs. The observed velocity dispersions are consistent with the dispersion in radial velocity derived for optically visible YSOs at the periphery of the cloud core and are consistent with virial equilibrium. The higher velocity dispersion of the YSOs in the plane of the sky relative to that of dense cores may be a consequence of stellar encounters between protostars due to a

Table 6
Dates and Integration Times of Observations

Julian Date	Field	Exposure Time (s)	Co-adds
2452066.8	1	30	40
2452069.8	2	20	60
2452070.8	3	20	60
2452071.8	4	5	240
2452072.8	4	5	240
2452417.8	1	20	40
2452418.9	2	10	120
2452423.8	3	10	120
2452446.8	4	5	240
2452450.7	1	10	120
2452454.7	2	10	120
2452455.7	3	10	120
2452769.9	1	5	240
2452770.8	2	5	240
2452771.9	3	5	240
2452775.8	4	5	240
2452800.8	1	5	240
2452801.8	2	5	240
2452813.8	4	5	240
2453105.9	4	5	240
2453107.9	3	5	240
2453108.9	1	5	240
2453127.9	2	5	240
2453132.9	4	5	240
2453135.8	2	5	240
2453136.8	1	5	240
2453152.8	3	5	240
2453153.8	1	5	240
2453567.7	1	5	240
2453579.7	3	5	240
2453834.0	4	5	240
2453835.0	3	5	240
2453838.9	4	5	240
2453841.9	2	5	240
2453861.9	2	5	240
2453870.9	1	5	240
2453871.9	2	5	240
2453889.8	1	5	240
2453892.8	3	5	240
2455689.9	1	5	240
2455693.9	4	5	240
2455694.9	3	5	240
2455696.9	2	5	240
2455697.9	1	5	240
2455717.8	3	5	240
2455718.8	4	5	240
2455721.8	2	5	240
2455722.8	3	5	240
2455725.7	1	5	240
2455728.7	4	5	240
2455729.8	2	5	240
2455758.7	2	5	240
2455780.7	3	5	240
2455794.6	1	5	240
2456046.9	4	5	240
2456047.9	4	5	240
2456048.9	3	5	240
2456050.9	2	5	240
2456052.9	1	5	240
2456053.9	4	5	240
2456054.9	3	5	240
2456060.9	2	5	240
2456061.9	1	5	240
2456080.8	1	5	240
2456081.8	2	5	240
2456082.8	3	5	240
2456083.8	4	5	240
2456087.8	1	5	240

global collapse of the L 1688 cloud core perhaps due to an external trigger or simply the formation of multiple stars in fragmenting dense cores and filaments.

An analysis of the differential magnitudes of objects over the 12 year baseline has not only confirmed the near-infrared variability for 29 YSOs established by prior studies, but also identified 18 new variability candidates. Four of these have not been previously identified as YSOs and may be newly identified cluster members.

We wish to thank H. Henden, C. Luginbuhl, J. Munn, and T. Tilleman for their various contributions to the USNO infrared parallax program, without which the astrometric observations would not have been possible. T.S. gratefully acknowledges support from a graduate fellowship from the NASA Missouri Space Grant Consortium. This research has made use of the NASA/IPAC Infrared Science Archive, which is operated by the Jet Propulsion Laboratory, California Institute of Technology, under contract with the National Aeronautics and Space Administration.

APPENDIX
DATES OF OBSERVATIONS

The Julian dates of observations and exposure times are presented in Table 6. Each entry typically represents three dithered images with 20 minutes of integration per dither.

REFERENCES

Alves de Oliveira, C., & Casali, M. 2008, A&A, 485, 155
André, P., Belloche, A., Motte, F., & Peretto, N. 2007, A&A, 472, 519
Barsony, M., Haisch, K. E., Marsh, K. A., & McCarthy, C. 2012, ApJ, 751, 22
Bate, M. R. 2009, MNRAS, 397, 232
Bate, M. R., Bonnell, I. A., & Bromm, V. 2003, MNRAS, 339, 577
Bonnell, I. A., Larson, R. B., & Zinnecker, H. 2007, in Protostars and Planets V, ed. B. Reipurth, D. Jewitt & K. Keil (Tucson, AZ: Univ. Arizona Press), 149
Bontemps, S., André, P., Kaas, A., et al. 2001, A&A, 372, 173
Chini, R. 1981, A&A, 99, 346
Clarke, C., & Pringle, J. E. 1993, MNRAS, 261, 190
Comeron, F., Rieke, G. H., Burrows, A., & Rieke, M. J. 1993, ApJ, 416, 185
Crutcher, R. M. 2012, ARA&A, 50, 29
Cutri, R. M., Skrutskie, M. F., van Dyk, S., et al. 2003, 2MASS All Sky Catalogue of Point Sources (The IRSA 2MASS All-Sky Point Source Catalog, NASA/IPAC Infrared Science Archive)
de Geus, E. J. 1992, A&A, 262, 258
Dolidze, M. V., & Arakelyan, M. A. 1959, SvA, 3, 434
Elias, J. H. 1978, ApJ, 224, 453
Elmegreen, B. G. 2007, ApJ, 668, 1064
Erickson, K. L., Wilking, B. A., Meyer, M. R., Robinson, J. R., & Stephenson, L. N. 2011, AJ, 142, 140
Fischer, J., Vrba, F. J., Toomey, D. W., et al. 2003, Proc. SPIE, 4841, 564
Foster, J. B., Cottaar, M., Covey, K. R., et al. 2015, ApJ, 799, 136
Gagné, M., Skinner, S., & Daniel, K. 2004, ApJ, 613, 393

Gong, H., & Ostriker, E. C. 2011, ApJ, 729, 120
Goodwin, S. P. 2013, MNRAS, 430, L6
Grasdalen, G. L., Strom, K. M., & Strom, S. E. 1973, ApJL, 184, L53
Greene, T. P., & Young, E. T. 1992, ApJ, 395, 516
Grosso, N., Montmerle, T., Bontemps, S., André, P., & Feigelson, E. 2000, A&A, 359, 113
Günther, H. M., Cody, A. M., Covey, K. R., et al. 2014, AJ, 148, 122
Guszejnov, D., & Hopkins, P. F. 2015, MNRAS, 450, 4137
Gutermuth, R. A., Megeath, S. T., Myers, P. C., et al. 2009, ApJS, 184, 18
Howell, S. B. 1989, PASP, 101, 616
Imanishi, K., Koyama, K., & Tsuobi, Y. 2001, ApJ, 557, 747
Kirk, H., Pineda, J., Johnstone, D., & Goodman, A. 2010, ApJ, 723, 457
Kobayashi, H., & Ida, S. 2001, Icar, 153, 416
Lada, C. J., & Lada, E. A. 2003, ARA&A, 41, 57
Loinard, L., Torres, R. M., Mioduszewski, A. J., & Rodriguez, L. F. 2008, in Proc. IAU Symp., 248, A Giant Step: from Milli- to Micro-arcsecond Astrometry, ed. W. J. Jin, I. Platais & M. A. C. Perryman (Dordrecht: Kluwer), 186
Lombardi, M., Lada, C. J., & Alves, J. 2008, A&A, 480, 785
Loren, R. B. 1989a, ApJ, 338, 902
Loren, R. B. 1989b, ApJ, 338, 925
Luginbuhl, C. B., Henden, A. A., Vrba, F. J., & Guetter, H. H. 1998, Proc. SPIE, 3354, 240
Mamajek, E. 2008, AN, 329, 10
Marsh, K. A., Kirkpatrick, J. D., & Plavchan, P. 2010a, ApJL, 709, L58
Marsh, K. A., Plavchan, P., Kirkpatrick, J. D., et al. 2010b, ApJ, 719, 550
Monet, D. G., Dahn, C. C., Vrba, F. J., et al. 1992, AJ, 103, 638
Motte, F., André, P., & Neri, R. 1998, A&A, 336, 150
Parks, J. R., Plavchan, P., White, R. J., & Gee, A. H. 2014, ApJS, 211, 3
Peretto, N., André, P., & Belloche, A. 2006, A&A, 445, 979
Pineda, J., Caselli, P., & Goodman, A. A. 2008, ApJ, 679, 481
Preibisch, T., & Zinnecker, H. 1999, AJ, 117, 2381
Proszkow, E.-M., & Adams, F. C. 2009, ApJS, 185, 486
Reipurth, B., Clarke, C. J., Boss, A. P., et al. 2014, in Protostars and Planets V, ed. H. Beuther et al. (Tucson, AZ: Univ. Arizona Press), 267
Rigliaco, E., Wilking, B., Meyer, M. R., et al. 2015, A&A, submitted
Rivera, J., Loinard, L., Dzib, S., et al. 2015, ApJ, 807, 119
Strom, K. M., Kepner, J., & Strom, S. E. 1995, ApJ, 438, 813
Struve, O., & Rudkjobing, M. 1949, ApJ, 109, 92
Tamura, M., Hashimoto, J., Kandori, R., et al. 2011, in ASP Conf. Ser., 449, Astronomical Polarimetry 2008: Science from Small to Large Telescopes, ed. P. Bastien et al. (San Francisco, CA: ASP), 207
Tobin, J. J., Hartmann, L., Furesz, G., Hsu, W.-H., & Mateo, M. 2015, AJ, 149, 119
Vrba, F. J. 1977, AJ, 82, 198
Vrba, F. J., Henden, A. A., Luginbuhl, C. B., et al. 2004, AJ, 127, 2948
Vrba, F. J., Strom, K. M., Strom, S. E., et al. 1975, ApJ, 197, 77
Vrba, F. J., Strom, S. E., & Strom, K. M. 1976, AJ, 81, 958
Wilking, B. A., Gagné, M., & Allen, L. E. 2008, in Handbook of Star Forming Regions, Vol. II, ed. B. Reipurth (San Francisco, CA: ASP), 351
Wilking, B. A., & Lada, C. J. 1983, ApJ, 274, 698
Wilking, B. A., Lada, C. J., & Young, E. T. 1989, ApJ, 340, 823
Wilking, B. A., Meyer, M. R., Robinson, J. G., & Greene, T. P. 2005, AJ, 130, 1733 AJ, 94, 106